Experimental and Linear Analysis for the Instability of Non-Newtonian Liquid Jets Issuing from a Pressurized Vibrating Nozzle

Cristina Rodríguez-Rivero, Eva M. M. Del Valle, and Miguel A. Galán
Chemical Engineering Dept., University of Salamanca, P/Los Caídos S/N 37008 Salamanca, Spain

DOI 10.1002/aic.14790
Published online March 27, 2015 in Wiley Online Library (wileyonlinelibrary.com)

The laminar capillary breakup of viscoelastic jets to produce polymeric microcapsules is analyzed experimentally and theoretically. The phenomenon is based on subjecting a capillary jet to controlled disturbances so that it eventually breaks up forming individual droplets. A dispersion relation from a temporal linear analysis to describe and predict the system behavior that includes the Oldroyd-B constitutive equation to take into account the viscoelasticity of the liquid is obtained. Dispersion curves relating growth rate and wavenumber of the perturbed jets are compared with experimental conditions and the chosen mathematical approach is found that fairly describes the system. The obtained dispersion relation eases the study of the effect of viscosity, elasticity, through relaxation times, and flow rate in the system. The approach allows finding the best conditions to obtain homogeneous droplets and describes the system qualitatively.
 AIChE J, 61: 2070–2078, 2015
Keywords: linear analysis, jet breakup, viscoelasticity, dispersion equation

Introduction

The instability of jets is a widely studied topic in Fluid Mechanics. One of its applications involves the production of droplets from the breakup of capillary jets issuing from nozzles. These droplets can be hardened, obtaining microcapsules. Our research group has made use of this method under different conditions to manufacture microparticles.[1–3] Particularly, we have focused on breakup techniques with medium-high viscosity non-Newtonian polymers, producing jets with the help of high pressure systems, whose instabilization is controlled and so their eventual breakup.

In this particular work, a polymeric solution is driven toward a capillary nozzle to form a jet whose instability is controlled by mechanical vibration, developing a Rayleigh-type jet breakup.

Savart, Plateau, Rayleigh, and Weber[4–7] studied the mechanisms of liquid jet stability and breakup from the last decades of the 19th century. After them, many researchers have shown an increasingly interest on the topic.[8–10] Most of the studies about jet disintegration depict instabilities in Newtonian fluids, and studies on non-Newtonian fluid jets are less found in the literature. However, it has long been known that the addition of polymers to a liquid affects the stability and consequently the breakup of jets due to their viscoelastic behavior.

Middleman, Goldin, and Bousfield[11–13] were the first authors to study the breakup of viscoelastic fluids. From their works and more recent studies,[14,15] we can conclude that there are differences in the way that viscoelastic and Newtonian fluids destabilizes. Viscoelasticity delays the onset of the disturbance growth but, at the same time, the growth becomes faster when the instability is developed. Moreover, the breakup length is both retarded and lengthened due to extensional stresses and clearly the patterns of deformation differ.

In previous studies,[3] we obtained a semiempirical model based on the wave-mechanism theory that describes, stemming from experimental relationships, the behavior of the system considering the flow velocity, zero-shear viscosity, and surface tension of the liquid solution.

The present work addresses the study of the jet instability through a more complete analysis in order to find the best conditions to make the process optimal, reliable, and predictable. The article collects a perspective of previous studies, describes the breakup process, includes the equations that develop the temporal linear analysis, and compares experimental data and dispersion equation results.

The main contribution will be the analysis of the effects of high zero-shear viscosities, different relaxation times assumptions, and different flow rate conditions. Whereas analyses in bibliography reach Ohnesorge numbers from 0.4 up to 2 in some cases, this study includes samples with Ohnesorge values from 10 to 25 due to high value of viscosity and low radii of the capillary nozzles.

Materials

The viscoelastic polymer used for this study was sodium alginate. It is a biocompatible and biodegradable

Current address of Cristina Rodríguez-Rivero: Department of Engineering, University of Cambridge, 17 Charles Babbage Road, CB3 0FS, Cambridge, U.K.

Correspondence concerning this article should be addressed to E. M. M. Del Valle at emvalle@usal.es.

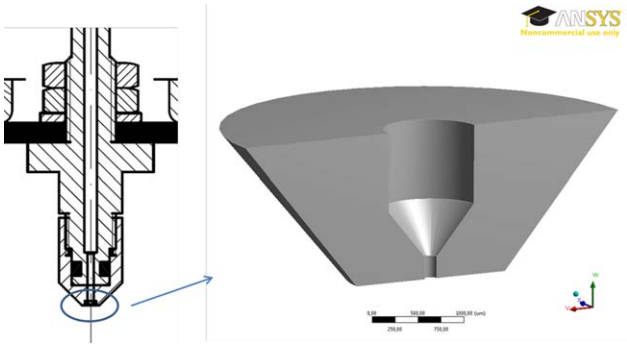

Figure 1. Sketch of the capillary nozzle and approximate 3-D model of the nozzle exit.

[Color figure can be viewed in the online issue, which is available at wileyonlinelibrary.com.]

polysaccharide extracted from algae. Its use as agent to produce biocompatible capsules is extended.[16,17]

Alginic acid sodium salt from brown algae classified as medium viscosity—viscosity ≥ 2000 cP for a 2% w/w (25°C) according to the manufacturer—was purchased from Sigma-Aldrich. The solutions comprising concentrations between 1.3 and 2.1% w/w were prepared by pouring and dissolving alginate powder in ultrapure water under hard stirring for 1.5 h. The density ρ of the fluid and its surface tension σ remain constant for the range of solutions studied with magnitudes of 1000 kg/m^3 and 0.076 N/m, respectively.

The rheological properties of the samples have been measured by a controlled stress rotational rheometer AR-1500 EX (TA Instruments, New Castle, DE) and a Capillary Breakup rheometer (CaBER, Thermo Haake GmbH, Karlsruhe, Germany) at 20°C. The parameters will be reported when needed.

Barium chloride dehydrated reagent grade purchased from Scharlau was used to prepare hardening solutions in a concentration 2% w/w.

A high-speed camera Phantom V310 (Vision Research Inc.) with two different lenses, 90 and 105 mm, was used to record experimental essays. Laser diffraction (Mastersizer 2000 particle size analyzer, Malvern Instruments Ltd., UK) was used to measure the microparticle diameters, which are given as Sauter mean diameter which accounts for the ratio volume/surface of spherical particles.

The nozzle has an inner geometry consisting of an initial 2-mm capillary, followed by a 1-mm capillary that leads to the final 150 μm capillary through a cone-shape reduction. The reduction from the 1-mm capillary to the exit of the nozzle is shown in Figure 1.

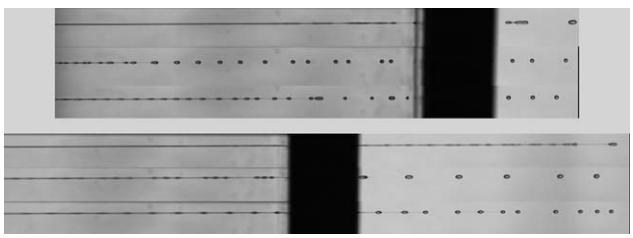

Figure 2. (a) Droplet formation for a 1.8% w/w solution–5 mL/min—applying different frequencies (0, 800, and 1400 Hz). (b) Droplet formation for a 1.8% w/w solution—7 mL/min—applying different frequencies (0, 800, and 1400 Hz).

Methodology

Description of the jet and breakup

This work involved an experimental approach and a subsequent theoretical study. The experimental methodology comprises recording the formation and evolution of jets and droplets under different conditions. The conditions selected were as follows. The liquid solution is forced by the application of a manometric pressure around 1–3 bar, which mean flow rate values from 5 to 8 cm^3/min, the viscosities go from 0.9 to 2.7 Pa s, the diameter of the capillary nozzle is 150 μm, and the recordings are taken at different distances from the nozzle around 3–5 cm downstream the exit.

These conditions are found to be the easiest to record and so analyzed. For further information about the system, refer to previous works.[1–3]

Figure 2 reveals different patterns developed by a jet of sodium alginate when it evolves naturally and when external mechanical vibrations of different frequencies are applied. Newtonian liquid jets show behaviors as those in Figure 3.

The patterns in Figure 2 show sinusoidal axisymmetric waves after the nozzle exit, turning into a bead on a string structure downstream. Beads of solution are then connected by thin ligaments or threads, and the breakup and size are determined by the behavior of the main droplets and ligaments.

Figure 2 provides information about the effects of the main parameters, namely viscosity, flow rate, and the applied external vibration frequency.

When the viscosity increases, for the same flow rate and similar wavenumbers, the breakup length increases considerably and the formation of droplets exhibits more irregularities or nonlinear effects. It should also be related to a shorter growth rate in the dispersion curves describing the perturbation profile in the jet.

When the flow rate increases, keeping a constant concentration and frequency applied, the breakup length increases. The growth rate obtained from the dispersion curves should also decrease with the flow rate for the same applied frequencies, which translates into shorter wavenumbers.

Finally, it is important to note that the range of frequencies that lead to the breakup of the jet is wide but not all frequencies lead to homogeneous microcapsules. Thus, an optimal range is observed in all cases and, in general, there is a minimum frequency from which the jet does not exhibit satellite droplets. We suggest that we could determine the best optimal conditions matching with this experimental range through a dispersion relation, relating wavenumber, and growth rate of the waves.

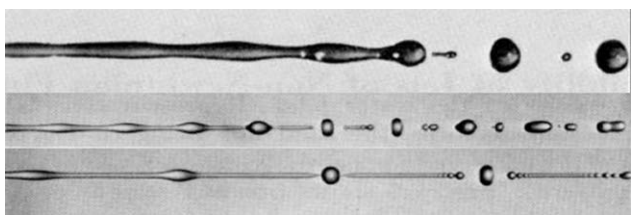

Figure 3. Breakup of Newtonian jets.

Theoretical Study

The mathematical approach adopted in this study comprised a temporal linear analysis. The common ways to tackle this type of instabilities are temporal or spatial and, in turn, linear or nonlinear. The temporal analysis considers solutions that are periodic in space and exponential in time, as observed for the process.

The linear analysis supposes that the disturbance initially shows a wave-like pattern with infinitesimal amplitude compared to its wavelength and the unperturbed jet radius. However, it has been checked that, for certain cases at low velocities, the prediction is still valid even when the amplitude increases considerable. This suggests that in certain cases the nonlinear terms in the momentum equations do not affect significantly the jet.[12]

The decision to focus on a linear approach instead of a nonlinear analysis is based on the results observed from experimentation. In all cases, the natural instability—not applying any external vibration—leads to uneven disturbances in terms of wavelength and amplitude, increasing in unevenness with the concentration. Conversely, when an external vibration from 600 Hz is applied, we observe waves with constant wavelengths, corresponding with the frequencies applied, and the obtained droplets are found regularly in distance. The amplitude of the perturbed jet seems to be growing exponentially on time (see Figure 2).

Thus, we considered that this pattern may be described by a temporal linear analysis. Hence, it could lead us to a dispersion equation that would indicate the wavelength of the disturbance that becomes in a faster growth for particular conditions. From this parameter also, the theoretical size of the resulting droplets could be predicted.

Our final objective is the assessment, by comparison with the experimental data, of whether the dispersion relation is appropriate to indicate the best conditions of breakup and, thus, also predict droplet sizes for these conditions. We do not try to describe the nonlinear effects such as the satellite droplet formation and migration.

Figure 4 shows a perturbed jet moving through an inviscid gas at a mean velocity $\overline{V}$ where the z axis is parallel and the x axis is normal to the flow. Some authors have already carried out linear temporal analyses considering the expressions and similar assumptions to those that we will address once again here.[19–21]

The way in which a jet evolves depends on the balance of forces acting on it. They are in general body forces (gravity, electromagnetic forces, and inertial effects), liquid pressure, stresses on the liquid—related mainly to the viscosity term—and surface tension.

The Bond number (1) gives us information about the pressure forces acting in the system. It relates hydrostatic pressure[22]—due to fluid weight—and Laplace contribution—linked to surface tension

$$\mathrm{Bo}=\frac{\rho\cdot g\cdot D^2}{\sigma} \tag{1}$$

With the properties of sodium alginate solutions and the approximated diameter of the jet $\mathrm{Bo}\approx 10^{-3}$ are obtained, indicating that surface tension forces dominate over gravitational effects and thus control the process. Therefore, we consider gravity forces negligible.

Regarding other physical assumptions, we neglect heat and mass transfer, consider the fluid incompressible, and assume constant surface tension along the jet. Gas inertia is also neglected as the density of the surrounding gas is negligible compared to the liquid density. Finally, we assume that the jet surface is perturbed in a symmetric way, with null velocity component in azimuthal direction.

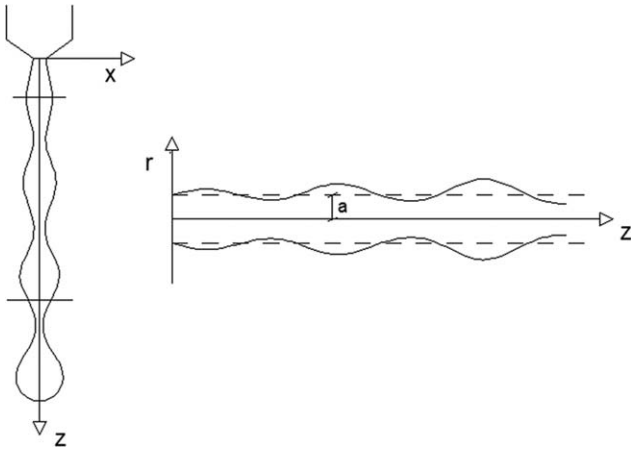

Figure 4. Schematic description of the coordinate system and basic parameters of the jet.

The analysis starts from the general equations of continuity and momentum

$$\frac{\partial\rho}{\partial t}+\nabla\cdot\rho\mathbf{v}=0 \tag{2}$$

$$\rho\left(\frac{\partial}{\partial t}+\mathbf{v}\cdot\nabla\right)\mathbf{v}=-\nabla\cdot\mathbf{T} \tag{3}$$

T is the total stress tensor of the liquid $\mathbf{T}=p\mathbf{I}+\tau$, p is the pressure of the fluid, $\boldsymbol{I}$ is the identity tensor, and τ is the viscous stress tensor or extra-stress tensor (also called stress deviatoric tensor).

Sodium alginate solutions exhibit non-Newtonian behavior, particularly viscoelastic, thus the analysis requires a non-Newtonian constitutive equation to account for the relationship between the viscous stresses and strain rate.

We consider one of the most general viscoelastic model, the corotational Oldroyd-B (4), whose constants are zero shear stress viscosity η_0 and time constants t_1 and t_2, relaxation and retardation times, respectively

$$\begin{aligned}&\boldsymbol{\tau}+t_1\frac{D\boldsymbol{\tau}}{Dt}-(\nabla\mathbf{v})^T\cdot\boldsymbol{\tau}-\boldsymbol{\tau}(\nabla\mathbf{v})\\&=2\eta_0\left[\mathbf{D}+t_2\frac{D\mathbf{D}}{Dt}-(\nabla\mathbf{v})\cdot\mathbf{D}-\mathbf{D}(\nabla\mathbf{v})^T\right]\\&\mathbf{D}=\frac{1}{2}\left\{\nabla\mathbf{v}+(\nabla\mathbf{v})^T\right\}\end{aligned} \tag{4}$$

Considering incompressible flow and linearizing the constitutive equation expressions, (2–4) become (5–7)

$$\nabla\cdot\mathbf{v}=0 \tag{5}$$

$$\rho\left(\frac{\partial}{\partial t}+\overline{V}\cdot\frac{\partial}{\partial z}\right)\mathbf{v}=-\nabla\cdot(p\mathbf{I}+\boldsymbol{\tau}) \tag{6}$$

$$\boldsymbol{\tau}+t_1\left(\frac{\partial}{\partial t}+\overline{V}\cdot\frac{\partial}{\partial z}\right)\boldsymbol{\tau}=-\eta_0\left[\dot{\boldsymbol{\gamma}}+t_2\left(\frac{\partial}{\partial t}+\overline{V}\cdot\frac{\partial}{\partial z}\right)\dot{\boldsymbol{\gamma}}\right] \tag{7}$$

where $\dot{\boldsymbol{\gamma}}$ is the shear strain rate tensor and $\overline{V}$ the average axial velocity of the fluid.

The destabilized cylindrical jet induces an axisymmetric wave in the surface of the fluid which applies to surface displacement but also velocities, stress and strain tensors, and pressure profiles.

The harmonic perturbations are of the form (8) according to a linear temporal analysis with varicose perturbation mode

$$r_s = a + A_0 e^{(\omega t + ikz)} \tag{8}$$

where a is the radius of the unperturbed jet, z is the axial component, ω is a complex frequency (its real part ω_r represents the growth rate of the disturbance and its imaginary part the frequency), t is time, A_0 is the amplitude of the perturbation at t_0, and k is the wave number.

The altered profiles for velocity, pressure, stress tensor, and strain rate tensor are described by (9–12), their amplitudes defined in uppercase

$$\mathbf{v} = \mathbf{V}(r) e^{(\omega t + ikz)},\ v_r = v_{r0} e^{(\omega t + ikz)},\ v_z = v_{z0} e^{(\omega t + ikz)} \tag{9}$$

$$p = P(r) e^{(\omega t + ikz)} \tag{10}$$

$$\boldsymbol{\tau} = \mathbf{T}(r) e^{(\omega t + ikz)} \tag{11}$$

$$\dot{\boldsymbol{\gamma}} = \dot{\mathbf{\Gamma}}(r) e^{(\omega t + ikz)} \tag{12}$$

Substituting expressions (11) and (12) into (7), the expression (13) is obtained

$$\tau = \eta(\omega)\dot{\gamma} \tag{13}$$

where

$$\eta(\omega) = \eta_0 \frac{1 + t_2\left(\omega + ik\overline{V}\right)}{1 + t_1\left(\omega + ik\overline{V}\right)} \tag{14}$$

These last expressions into (5) and (6), expressed in cylindrical coordinates, lead to the partial differential Eqs. (PDEs) 15–17

$$\frac{1}{r}\frac{\partial}{\partial r}(r v_r) + \frac{\partial v_z}{\partial z} = 0 \tag{15}$$

$$\rho\left(\frac{\partial v_r}{\partial t} + \bar{V}\frac{\partial v_r}{\partial z}\right) = -\frac{\partial p}{\partial r} + \eta(\omega)\left[\frac{\partial}{\partial r}\left(\frac{1}{r}\frac{\partial}{\partial r}(r v_r)\right) + \frac{\partial^2 v_r}{\partial z^2}\right] \tag{16}$$

$$\rho\left(\frac{\partial v_z}{\partial t} + \bar{V}\frac{\partial v_z}{\partial z}\right) = -\frac{\partial p}{\partial z} + \eta(\omega)\left[\frac{1}{r}\frac{\partial}{\partial r}\left(r\frac{\partial v_z}{\partial r}\right) + \frac{\partial^2 v_z}{\partial z^2}\right] \tag{17}$$

The PDEs are reduced to ordinary differential equations (ODEs) by substituting (9) and (10) into (15–17). The ODEs are of the form of Bessel functions with respect to the variable r.

The boundary conditions here considered at the gas-liquid interface to solve the system of ODEs were already applied by Tomotika[23] and are as follows. The kinematic condition or no slipping condition at the surface of the jet (18) requires that the velocity components are continuous at the surface. The dynamic boundary conditions (19) and (20) define the tangential stress parallel to the surface as continuous at the surface of the column and relate the difference in the normal stress between the inside and outside of the column to the interfacial surface tension

$$v_r = \left(\frac{\partial}{\partial t} + \overline{V}\cdot\nabla\right)\left(A_0 e^{(\omega t - jkz)}\right) \tag{18}$$

$$\mathbf{T}\times\mathbf{n} = 0 \tag{19}$$

$$\mathbf{T}\cdot\mathbf{n} + \sigma\nabla\cdot\mathbf{n} = 0 \tag{20}$$

Expressions (21–25) result from linearizing and defining parameters in (19) and (20)

$$v_r = \left(\frac{\partial\left(A_0 e^{(\omega t - jkz)}\right)}{\partial t} + \overline{V}\cdot\frac{\partial\left(A_0 e^{(\omega t - jkz)}\right)}{\partial z}\right) \qquad r = a \tag{21}$$

$$T_{rz} = \tau_{rz} = -\eta(\omega)\left(\frac{\partial v_z}{\partial r} + \frac{\partial v_r}{\partial z}\right) = 0 \qquad r = a \tag{22}$$

$$T_{rr} + p_\sigma = 0 \qquad r = a \tag{23}$$

where

$$T_{rr} = p + \tau_{rr} = p - 2\eta(\omega)\frac{\partial v_r}{\partial r} \tag{24}$$

$$p_\sigma = \frac{\sigma_0}{a^2}\left(A_0 e^{ikz+\omega t} + a^2\frac{\partial^2\left(A_0 e^{ikz+\omega t}\right)}{\partial z^2}\right) = \frac{\sigma_0}{a^2}\left(1 - a^2k^2\right)A_0 e^{ikz+\omega t} \tag{25}$$

Profiles (26–28) are obtained after solving the system of ODEs, where I_0 and I_1 are modified Bessel functions of the first kind

$$v_r = \left[\frac{l^2+k^2}{I_1(ka)}I_1(kr) - \frac{2k^2}{I_1(la)}I_1(lr)\right]\frac{\eta(\omega)}{\rho}A_0 e^{(\omega t - jkz)} \qquad r \le a \tag{26}$$

$$v_z = i\left[\frac{l^2+k^2}{I_1(ka)}I_0(kr) - \frac{2kl}{I_1(la)}I_0(lr)\right]\frac{\eta(\omega)}{\rho}A_0 e^{(\omega t - jkz)} \qquad r \le a \tag{27}$$

$$p = \frac{l^2+k^2}{kI_1(ka)}I_0(kr)\eta(\omega)\left(\omega + ik\overline{V}\right)A_0 e^{(\omega t - jkz)} \qquad r \le a \tag{28}$$

where

$$l^2 = k^2 + \frac{\rho\left(\omega + ik\overline{V}\right)}{\eta(\omega)} \tag{29}$$

The normal stress T_{rr} in the liquid is obtained from substituting the corresponding equations of velocity and pressure profiles into (24)

$$T_{rr} = -\left\{\frac{l^2+k^2}{I_1(ak)}\left[\frac{\rho}{k}\left(\omega + ik\overline{V}\right)I_0(kr) + 2k\eta(\omega)I_1'(kr)\right] - \frac{4k^2 l\eta(\omega)}{I_0(la)}I_1'(lr)\right\}\frac{\eta(\omega)}{\rho}A_0 e^{(\omega t + ikz)} \tag{30}$$

The dispersion equation 31 is obtained when expressions (25) and (30) are introduced to define the normal stress boundary condition (23)

$$\omega^2\frac{ak}{2}\frac{I_0(ak)}{I_1(ak)} + \omega\frac{\eta_0}{\rho a^2}\frac{1 + \lambda_2\left(\omega + ik\overline{V}\right)}{1 + \lambda_1\left(\omega + ik\overline{V}\right)} + k^2a^2\left[2ak\frac{I_0(ak)}{I_1(ak)}\frac{l^2}{l^2-k^2} - 1 - 2al\frac{I_0(al)}{I_1(al)}\frac{k^2}{l^2-k^2}\right] = \frac{\sigma k^2 a^2}{2\rho a^3}\left(1 - k^2a^2\right) \tag{31}$$

Expression (32) comes from taking the real part and rearranging terms in (31)

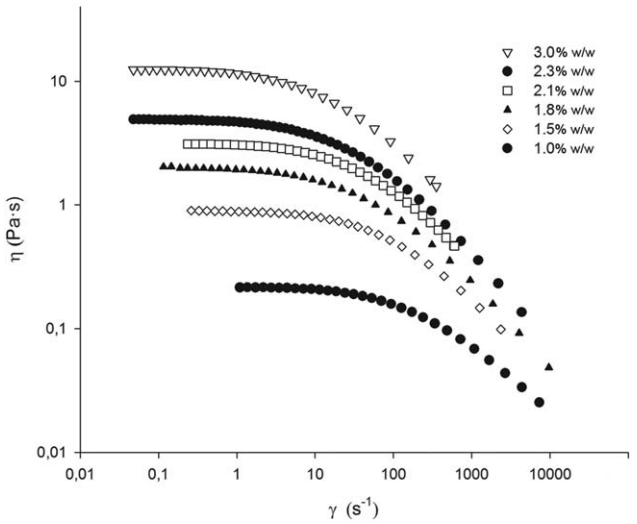

Figure 5. Flow curves of Na-Alg solutions.

Viscosity as a function of shear rate.

$$\omega_r^2 \frac{ak}{2}\frac{I_0(ak)}{I_1(ak)} + \omega_r \frac{\eta(\omega)}{\rho}$$
$$k^2\left[2ak\frac{I_0(ak)}{I_1(ak)}\frac{l^2}{l^2-k^2} - 1 - 2al\frac{I_0(al)}{I_1(al)}\frac{k^2}{l^2-k^2}\right] = \quad (32)$$
$$= \frac{\sigma k^2 a^2}{2\rho a^3}\left(1-k^2a^2\right)$$

The expression is adimensionalized (37) using a ratio of deformation retardation time to stress relaxation time $\bar{t}=t_2/t_1$ (time ratio), the Ohnesorge number which denotes the ratio of viscous force to surface tension force

$$Z = \frac{\eta_0}{\sqrt{\rho\sigma a}} \quad (33)$$

El, known as elasticity number,[24] that represents a relationship between viscous effect and elastic effect in the fluid

$$\mathrm{El} = \frac{t_1 \cdot \eta_0}{\rho \cdot a^2} \quad (34)$$

Ω_r is the nondimensional growth rate

$$\Omega_r = \frac{\omega_r}{\sqrt{\sigma/(\rho a^3)}} \quad (35)$$

and al can be expressed in dimensionless form by prior parameters as

$$al = \sqrt{(ak)^2 + \frac{\Omega_r}{Z}\frac{Z+El\cdot\Omega_r}{Z+\bar{t}El\cdot\Omega_r}} \quad (36)$$

$$\left[Z\frac{Z+\bar{t}\cdot\mathrm{El}\cdot\Omega}{Z+\mathrm{El}\cdot\Omega}\right]^2\left\{2(ak)^2\left[1-\left(\frac{al}{ak}\right)^2\right]\right.$$
$$\left.+(ak)^3\left[1+\left(\frac{al}{ak}\right)^2\right]^2\frac{I_0(ak)}{I_1(ak)} - 4(ak)^2(al)\frac{I_0(al)}{I_1(al)}\right\} = 1-(ak)^2 \quad (37)$$

Rheological characterization

The dispersion relation includes rheological parameters, η_0, t_1, and t_2, which involves the need to carry out rheological tests. In general, polymer solutions behave as non-Newtonian fluids and exhibit a viscosity depending strongly on the shear stress or strain rate. In particular, most polymeric solutions exhibit a viscoelastic behavior, which means that they display viscous but also elastic effects.[25,26]

Table 1. Rheological Parameters Obtained by Fitting Data to the Cross Equation

c (g/dL)	η_0 (Pa s)	λ_C (s)	m	Z
1.5	0.911	7.66×10^{-3}	0.759	11.33
1.8	2.032	0.0169	0.722	25.28
2.0	2.744	0.0175	0.758	34.14
2.3	4.953	0.0259	0.744	61.62
3.0	12.70	0.0481	0.730	158.01

Flow curves give us information about a characteristic zero-shear viscosity and a measure of relaxation time. The Cross model[27] (38) resulted in the generalized Newtonian model that better fitted the data for all alginate solutions tested

$$\eta = \eta_\infty + \frac{\eta_0-\eta_\infty}{1+(\tau_1\cdot\dot{\gamma})^m} \quad (38)$$

where η is the apparent shear viscosity, η_0 is the zero-shear rate viscosity or Newtonian viscosity, η_∞ is the infinite viscosity, τ_1 is the Cross time constant or relaxation time under shear conditions, $\dot{\gamma}$ is the strain rate, and m the Cross or flow behavior index. m indicates the degree of dependence of viscosity on shear rate in the shear-thinning region, the more close to the unit the more non-Newtonian behavior.

Figure 5 and Table 1 collect the value of the rheological parameters from the fitting to (38). Infinite shear viscosity values, η_∞, have been omitted because the extrapolation to such values cannot be validated by the experimental data and these values are not needed for the rest of the analysis.

Stress relaxation time

Stress relaxation time can also be determined by small amplitude oscillatory shear (SAOS) measurements and extensional flow measurements. Different external fields are applied in each case.

The characteristic stress relaxation time for SAOS can be typically considered as the inverse of the frequency value at the cross point between the storage and loss modules, G' and G'', respectively.[28,29] However, we could not rely on the values obtained in that way due to inertial effects of the rheometer. We then estimated the relaxation times from the crossover frequency extrapolated from the terminal behavior of G' and G'' with Slopes 2 and 1, respectively, which make the values higher than expected.

Conversely, the relaxation times from uniaxial extensional flow measurements were obtained using a CaBER rheometer by applying expression (39)[30] to the evolution of the midpoint of a stretched ligament. It determines the growth characteristic scale of elastic stresses in the necking filament

$$\frac{R_{\mathrm{mid}}(t)}{R_0} = \left(\frac{GR_0}{2\sigma}\right)^{1/3}\exp\left[-t/3\tau\right] \quad (39)$$

where R_0 is the radius after the stretching of the filament finishes, τ is the so-called stress relaxation time, G is known as the relaxation modulus and refers to the value of the linear stress-relaxation function $G(t)$ when the material is subjected

Table 2. Characteristic Relaxation Times Obtained from Simple Shear, SAOS and Uniaxial Extensional Fields

c (g/dL)	η_0 (Pa s)	$t_{1,\mathrm{SHEAR}}$ (s)	$t_{1,\mathrm{SAOS}}$ (s)	$t_{1,\mathrm{CaBER}}$ (s)
1.5	0.911	7.66×10^{-3}	0.032	0.0157
1.8	2.032	0.0169	0.078	0.0330[a]
2.0	2.744	0.0175[a]	0.080[a]	0.0410
3.0	12.70	0.0481	0.350	0.0703

[a]Data have been extrapolated.

to a particular shear spectrum,[31] σ is the surface tension, and ρ the density.

Table 2 contains characteristic relaxation times obtained after applying the three different types of methods described. Compared with similar studies, the characteristic relaxation times obtained are one order of magnitude higher than those found for other polymeric systems, although the viscosities in this study are higher.[18,24] Wloka et al.[32] studied extracellular polymeric substances obtaining a lifetime of junction points of 17 ms.

Deformation retardation time

The obtaining of satisfactory data for the characteristic deformation retardation times through creep analyses was not possible to achieve. The larger viscous nature of the samples compared to the elastic response for low strain rates precluded us from obtaining satisfactory data. Hence, we turned to considerations found in the literature. For instance Bird et al.[33] conclude from the analysis of linear viscoelastic models that the ratio between retardation and relaxation time is less than the unit. In most studies, the retardation time is considered 10 times less than the relaxation times.[18,19,24] We assume the same consideration, so the adimensional parameter $\bar{t}=t_2/t_1=0.1$.

Results: Study of the Dispersion Equation

Data obtained experimentally showed certain patterns and behaviors as we detailed before (see Figure 2). From these data, we determined concurrently the relaxation time that best defines the behavior of the system and whether the predicted and experimental conditions are in good agreement.

Authors aforementioned[19,20] have checked the applicability of this theoretical dispersion relation in the disintegration of viscoelastic liquids jets at small Weber and Ohnesorge numbers. The formation of bending instabilities on the jets appear when Weber numbers exceed the order of 10^3 [14] and axisymmetric disturbances are not developed in the jet anymore, invalidating the obtained dispersion relation. However, no limitations related to high Ohnesorge numbers have been found. We will check the applicability of the expression for maximum values of Weber number around 150 and Ohnesorge values up to 25.

We used Mathematica® software to solve and plot the adimensional growth rate Ω as a function of wavenumber k. These two variables are in implicit form (37), hence we used Newton's method to estimate the maximum value of the function where the condition of null derivative is imposed.

To determine the theoretical size of droplets, for the fastest growth rate or any other condition, we apply the definition of wavenumber $k=\frac{2\pi}{\lambda}$ to obtain the wavelength from any k given by the dispersion relation (37). The estimated droplet size can be then computed as the diameter of a sphere whose volume is that of a cylinder having a length equal to the wavelength so that $\frac{4}{3}\pi r_{\mathrm{d}}^3=\pi r_{\mathrm{j}}^2\lambda$ where subscripts d and j indicates droplet and jet, respectively. Frequencies can be computed as $f=\frac{v_{\mathrm{j}}}{\lambda}$.

In set-up studies and for the previous published work,[3] we considered the expression obtained by Weber[7] to compute an "optimal" frequency to impose at the nozzle (40). We will compare Weber's wavelengths or frequencies and data from the dispersion relation in next sections

$$\lambda_{\mathrm{opt}}=\pi\cdot\sqrt{2}\cdot d\left(1+\frac{3\eta}{\sqrt{\rho\sigma\cdot d}}\right)^{1/2} \tag{40}$$

where d is the jet diameter.

Relaxation time effect

We have three different values of the relaxation time for every concentration. It is not clear how the relaxation times are determined in similar papers for the computation of the curves. Therefore, we first check the effect of the different magnitudes on the results and compare with the experimental data.

As for the stresses in the solution, both high shear stresses (mainly in the nozzle) and normal stresses are developing in the jet, however, the stretching or extensional effect keeps further downstream the nozzle and is expected to control the breakup process. Therefore, we expected to find the best agreement for the relaxation time from extensional measurements.

Pearson already suggested that the pronounced molecular orientation that arises in uniaxial extension was the protagonist of the different effects in jets. He also reported that the orientation of the molecules in uniaxial extension relaxes more slowly than orientation due to simple shear.[34] The way the flow develops in the nozzle is of major importance. A sudden contraction near the exit of the nozzle will

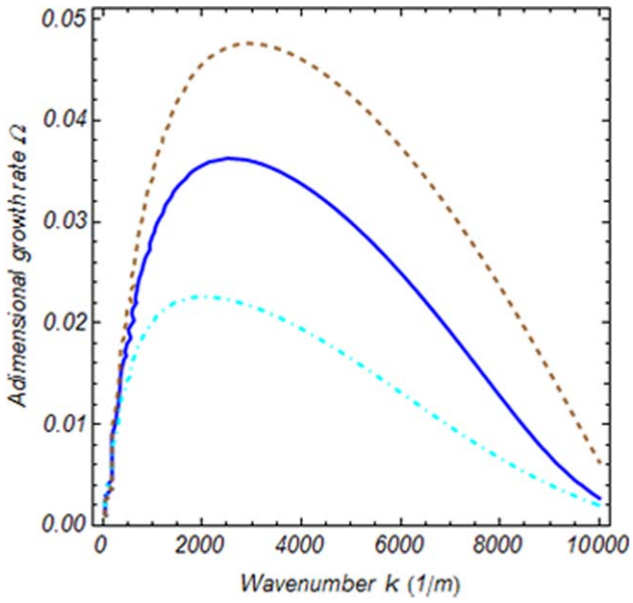

Figure 6. Dispersion curves for different relaxation times.

Sample of 1.8% w/w at 6 mL/min. Relaxation times obtained by SAOS (dashed line), CaBER (thick line), and simple shear (dot-dashed line). [Color figure can be viewed in the online issue, which is available at wileyonlinelibrary.com.]

Table 3. Predicted and Experimental Values for the Optimal Wavenumber, Wavelength, Droplet Size, Frequencies, and Final Microparticle Size for the different Relaxation Times Obtained for 1.8 g/dL Solution at 6 mL/min

	$t_{1,SHEAR}$ (s)	$t_{1,CaBER}$ (s)	$t_{1,SAOS}$ (s)
t_1 (s)	0.017	0.033	0.080
k (m^{-1})	2034	2577	2952
Ω	0.023	0.036	0.047
λ (m)	0.0076	0.0024	0.0021
Size (μm)	523	483	462
Frequency	1335	1691	1938
Exp. size		≈540	
Exp. frequency		1500–1800	

produce a profound uniaxial extensional flow combined with shear flow. A long capillary will lead to a fully developed shear profile. In both cases, the relaxation behaviors are different.

Figure 6 and Table 3 reveal the influence of the relaxation time on the growth rate for a 1.8% w/w solution and 6 cm^3/min flow rate. We considered a retardation time t_2 10 times less than the relaxation time t_1. We observe that the higher the relaxation time the higher the growth rate and the optimal wavenumber k, so it is the optimal frequency.

As said before, the best experimental conditions are found for an enclosed range of frequencies. Within this range, the obtained microcapsules are more homogeneous.

From the results in Figure 6 and Table 3, we propose that the data obtained from the extensional relaxation time are in a better agreement with the experimental conditions. Besides, this conclusion matches what was expected. Therefore, we will consider the extensional relaxation time for the rest of the study.

Regarding the difference between droplet size and microparticle size, we have observed a swelling of the structure when it solidifies in the gelling bath. We do not have particular studies on the topic.

Concentration effect

A variation in concentration means a variation in viscosity. The effect of viscosity in the dispersion curves can be easily assessed as shown in Figure 7. It reveals a pronounced decrease in the dimensionless growth rate when the viscosity increases. The viscous forces oppose to the growth of the capillary instability, causing also a lengthening of the breakup length. At the same time, k decreases when viscosity increases. This will cause bigger droplets under the predicted optimal conditions, which agrees with experimental data.

Table 4 reveals that the unique optimal Weber's wavelength values for every viscosity are larger than the optimal theoretical ones. This also involves that theoretical optimal frequencies are larger than Weber's dominant frequencies. With Weber conditions, the predicted droplet diameters are larger than the theoretical and experimental data.

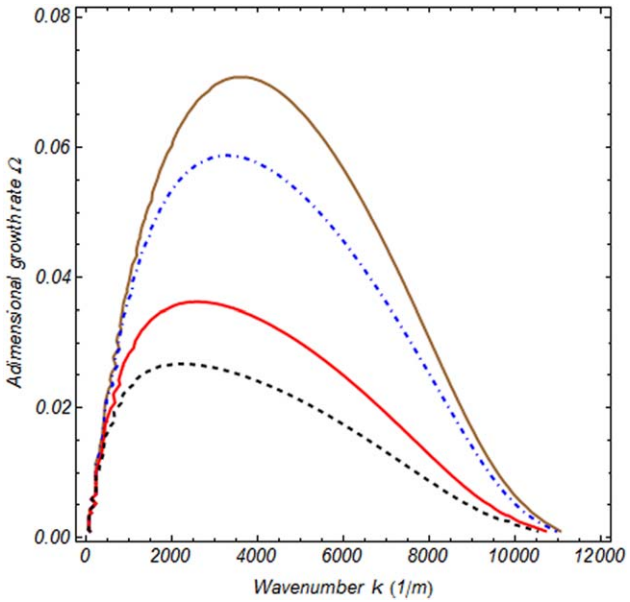

Figure 7. Dispersion curves for different concentrations keeping a constant flow rate (6 mL/min): 1.5% w/w (thick line), 1.6% w/w (dot-dashed line), 1.8% w/w (thick line), and 2% w/w (dashed line).

[Color figure can be viewed in the online issue, which is available at wileyonlinelibrary.com.]

Flow rate effect

The flow rate has been the most difficult parameter to assess. A change in the flow rate directly affects the velocity of the jet but also its diameter. Whereas the velocity is not directly involved in the dispersion equation (37) the variation of the jet radius directly affects it. Inset in Figure 8 displays the jet radii as function of flow rate for 1.6, 1.8, and 1.9% w/w. It indicates that, for this range of concentrations, the diameters remains constant for the same flow rates.

Figure 8 plots dispersion curves for different flow rates keeping a constant concentration of 1.6% w/w. We observed for all solution a shift toward higher wavenumbers when the flow rate increases, involving higher optimal frequencies. This tendency agrees with the experimental measurements. Thus, we check through the images that the best conditions are achieved where the dominant conditions in the curve are given.

Data in Table 5 show that an increase in the liquid flow rate destabilizes the jet, maximum Ω increases. We have observed that, in general for the optimal conditions, the breakup length remains almost constant (particularly for low flow rates, see Figure 9) or it increases with the flow rate. Therefore, it seems that there is a disagreement between the predicted growth rate and the experimental breakup length. A further study on this issue is needed.

Table 4. Predicted Optimal Parameters: From the Weber Expression (We), the Dispersion Relation (Th), Compared to the Experimental Parameters (Exp)

Conc. (g/dL)	λ_{We} (mm)	λ_{Th} (mm)	Ω (s^{-1})	f_{We} (s^{-1})	f_{Th}(s^{-1})	f (s^{-1})	$Size_{We}$ (μm)	$Size_{Th}$ (μm)	$Size_{Exp}$ (μm)
1.50	3.85	1.76	750.3	1070	2365	2100–2500	563	432	538
1.60	4.52	1.92	622.3	913	2153	1900–2200	594	446	562
1.80	5.72	2.44	383.8	721	1691	1500–1800	642	483	601
2.00	6.63	2.84	283.4	622	1453	1200–1500	675	508	625

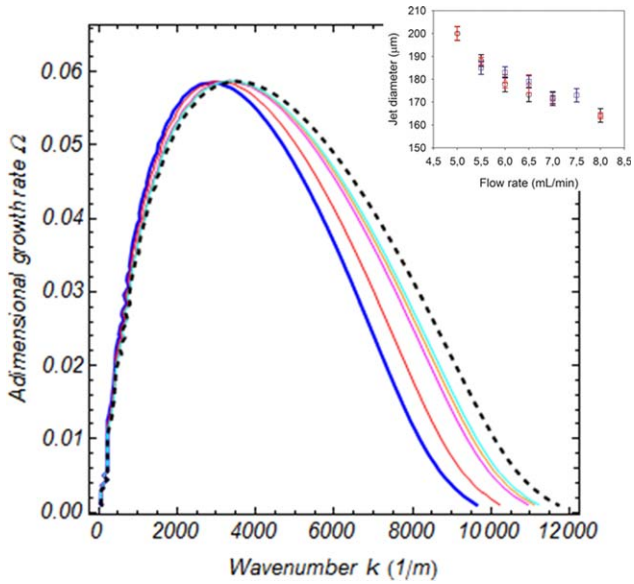

Figure 8. Adimensional growth rate as a function of wavenumber for a 1.6% w/w alginate solution under different flow rates.

Lowest flow rate in thick line—5 mL/min, highest flow rate in dashed line—8 mL/min. Inset: Effect of flow rate on the jet diameter. [Color figure can be viewed in the online issue, which is available at wileyonlinelibrary.com.]

Conclusions

Prior studies by the authors concerning the addressed mechanism of jet breakup were based on a semiempirical approach. Therefore, the behavior of the system remained not completely described. We have proposed in this work a more complete mathematical approach through a linear analysis. It accounts for viscoelastic effects that were not considered previously.

From the results, we conclude that the proposed approach is valid for describing the jet breakup mechanism of medium-viscosity viscoelastic polymers. On one hand, it allows predicting the optimal range of frequencies to achieve homogeneous samples. On the other hand, it reveals the effects that most influence the system behavior through the comparison of the curves with the experimental data.

We could verify that elastic effects rule over simple shear effects through the assessment of different magnitudes of relaxation time, obtained from different flow field measurements. However, we have to be aware of the advances that the rheological characterization for complex processes such as jet instabilities are experiencing nowadays. As an example, common oscillatory shear measurements are based on essays applying low shear stress measurements (SAOS). A new technique that superposes an oscillatory motion onto a steady-state shear flow—orthogonal and parallel superposition—is shredding light into the combination of these flow fields. Thus, several authors[35,36] have demonstrated that increasing the steady-state shear rate, the crossover of storage and loss moduli G' and G'', shifts to higher frequencies. The relaxation times are rate dependent. This could lead to the determination of new constitutive equations.

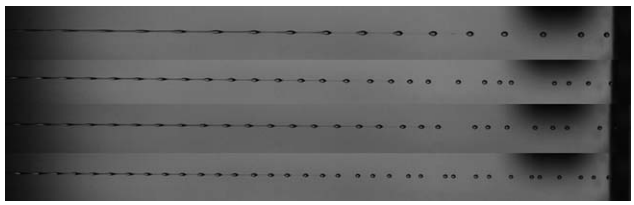

Figure 9. Theoretical optimal breakup conditions for jets of 1.6% w/w alginate solution under different flow rates—5, 5.5, 6, and 6.5 mL/min.

The equation used in this work, Oldroyd-B, has resulted appropriate for the range of concentrations studied. The use of other constitutive equations might be also adequate and interesting to evaluate, particularly when a wider range of concentrations are studied.

As for the droplet size obtained, it results less than the measured size of the final microparticles. This suggests that there is a swelling mechanism to be further described. Furthermore, it is worth saying that the correct and up-to-date determination of the flow rate, rheological characterization, and experimental conditions is of great importance when the experiments are being carried out. Slight differences in the data introduced in the dispersion relation leads to important differences in the results.

For future works, it is of highly interest to study nonlinear inertial terms and analyse the nonlinearity of the viscoelasticity through nonlinear approaches. It would help to describe the system further, for instance the satellite droplet formation.

Besides, it would also be of high interest to find a relationship between the growth rate and breakup length.

Acknowledgments

This research was supported by funds from the European Reseach Council through the project "Development of a technology to produce microcapsules based on the formation of drops from viscous non-Newtonian liquids sprayed through fan-jet nozzles to use in cancer therapy" (ERC-2010-StG_20091028), with PR Eva Martin Del Valle. The authors gratefully acknowledge the financial support. Cristina Rodríguez-Rivero was supported by a F.P.U. fellowship from the Minister of Education of Spain, which is gratefully acknowledged by the authors.

Table 5. Optimal Wavenumber, Growth Rate, Frequency, and Size Applying Different Flow Rates for a 1.6 g/dL solution

Q (mL/min)	λ_{We} (mm)	λ_{Th} (mm)	Ω (s^{-1})	f_{We} (s^{-1})	f_{Th} (s^{-1})	f (s^{-1})	$Size_{We}$ (μm)	$Size_{Th}$ (μm)	$Size_{Exp}$ (μm)
5	4.98	2.18	511	533	1215	1100–1300	669	508	–
5.5	4.76	2.05	561	693	1607	1500–1700	633	478	538
6	4.52	1.92	622	913	2154	1900–2200	594	446	512
6.5	4.47	1.88	647	1029	2449	2400–2600	586	440	503
7	4.43	1.87	645	1141	2705	2700–2900	580	435	506
8	4.29	1.79	688	1376	3296	3200–3500	558	417	473

Literature Cited

1. Cerveró JM, Nogareda J, Valle EMMD, Galán MA. Development of a technology to produce monodispersed microparticles based on the formation of drops from viscous non-Newtonian liquids sprayed through a fan jet nozzle. *Chem Eng J*. 2011;174(2–3):699–708.
2. Herrero EP, Martín Del Valle EM, Galán MA. Development of a new technology for the production of microcapsules based in atomization processes. *Chem Eng J*. 2006;117(2):137–142.
3. Rodríguez-Rivero C, Del Valle EMM, Galán MA. Development of a new technique to generate microcapsules from the breakup of non-Newtonian highly viscous fluid jets. *AIChE J*. 2011;57(12):3436–3447.
4. Savart F. Mémoire sur la constitution des veines liquides lancées par des orifices circulaires en mince paroi. *Ann Chim.* 1833;53:337–386.
5. Plateau J, editor. Statique expérimentale, théorique des liquides soumis aux seules forces moléculaires. Paris: Gauthier-Villars, 1873.
6. Rayleigh L. On the capillary phenomena of jets. *Proc R Soc London.* 1879;29:71–97.
7. Weber C. Zum Zerfall eines Flüssigkeitsstrahls. *Z Angew Math Mech.* 1931;11:136.
8. Goedde EF, Yuen MC. Experiments on liquid jet instability. *J Fluid Mech.* 1970;40(3):495–511.
9. Bogy DB. Drop formation in a circular liquid jet. *Annu Rev Fluid Mech.* 1979;11(1):207–228.
10. Chigier N, Reitz R.D. Regimes of jet breakup and breakup mechanisms- Physical aspects. In Recent advances in spray combustion: Spray atomization and drop burning phenomena. 1. 1996:109–136. Ed. K. K. Kuo. AIAA, Reston, VA: American Institute of Aeronautics and Astronautics Inc.
11. Middleman S. Stability of a viscoelastic jet. *Chem Eng Sci.* 1965; 20(12):1037–1040.
12. Goldin M, Yerushalmi J, Pfeffer R, Shinnar R. Breakup of a laminar capillary jet of a viscoelastic fluid. *J Fluid Mech.* 1969;38(4):689–711.
13. Bousfield DW, Keunings R, Marrucci G, Denn MM. Nonlinear analysis of the surface tension driven breakup of viscoelastic filaments. *J Non-Newton Fluid Mech.* 1986;21(1):79–97.
14. Yarin AL. Free Liquid Jets and Films: Hydrodynamics and Rheology. Longman (in USA, Wiley), New York, 1993.
15. Christanti Y, Walker LM. Surface tension driven jet break up of strain-hardening polymer solutions. *J Non-Newton Fluid Mech.* 2001;100(1–3):9–26.
16. DeGroot AR, Neufeld RJ. Encapsulation of urease in alginate beads and protection from [alpha]-chymotrypsin with chitosan membranes. *Enzyme Microb Technol.* 2001;29(6–7):321–327.
17. Koch S, Schwinger C, Kressler J, Heinzen C, Rainov NG. Alginate encapsulation of genetically engineered mammalian cells: comparison of production devices, methods and microcapsule characteristics. *J Microencapsul: Micro Nano Carriers.* 2003;20(3):303–316.
18. Gordon M, Yerushalmi J, Shinnar R. Instability of jets of non-Newtonian fluids. *Trans Soc Rheol*. 1973;17(2):303–324.
19. Brenn G, Liu Z, Durst F. Linear analysis of the temporal instability of axisymmetrical non-Newtonian liquid jets. *Int J Multiphase Flow*. 2000;26(10):1621–1644.
20. Gao Z. Instability of non-Newtonian jets with a surface tension gradient. *J Phys A Math Theor*. 2009;42(6):065501.
21. Liu Z, Liu Z. Linear analysis of three-dimensional instability of non-Newtonian liquid jets. *J Fluid Mech.* 2006;559:451–459.
22. Gennes P-GD, Brochard-Wyart F, Quere D, editors. *Capillarity and Wetting Phenomena: Drops, Bubbles, Pearls, Waves*. New York: Springer, 2004.
23. Tomotika S. On the instability of a cylindrical thread of a viscous liquid sorrounded by another viscous fluid. *Proc R Soc London A*. 1935;150(870):322–337.
24. Kroesser FW, Middleman S. Viscoelastic jet stability. *AIChE J*. 1969;15(3):383–386.
25. Tian XY, Li MG, Cao N, Li JW, Chen XB. Characterization of the flow behavior of alginate/hydroxyapatite mixtures for tissue scaffold fabrication. *Biofabrication*. 2009;1(4):045005.
26. Muller FL, Davidson JF. Rheology of shear thinning polymer solutions. *Ind Eng Chem Res.* 1994;33(10):2364–2367.
27. Cross MM. Rheology of non-Newtonian fluids: a new flow equation for pseudoplastic systems. *J Colloid Sci*. 1965;20(5):417–437.
28. Huldén M. Hydrophobically modified urethane–ethoxylate (HEUR) associative thickeners 1. Rheology of aqueous solutions and interactions with surfactants. *Colloids Surf A Physicochem Eng Asp*. 1994; 82(3):263–277.
29. Tzoganakis C. A rheological evaluation of linear and branched controlled-rheology polypropylenes. *Can J Chem Eng*. 1994;72(4): 749–754.
30. Stelter M, Brenn G, Yarin AL, Singh RP, Durst F. Investigation of the elongational behavior of polymer solutions by means of an elongational rheometer. *J Rheol*. 2002;46(2):507–527.
31. Entov VM, Hinch EJ. Effect of a spectrum of relaxation times on the capillary thinning of a filament of elastic liquid. *J Non-Newton Fluid Mech.* 1997;72(1):31–53.
32. Wloka M, Rehage H, Flemming HC, Wingender J. Rheological properties of viscoelastic biofilm extracellular polymeric substances and comparison to the behavior of calcium alginate gels. *Colloid Polym Sci*. 2004;282(10):1067–1076.
33. Bird RB, Armstrong RC, Hassager O, editors. *Dynamics of Polymeric Liquids: Fluid Mechanics*, Vol. 1, 2nd ed. Wiley, New York, 1987.
34. Pearson JRA. Instability in Non-Newtonian flow. *Annu Rev Fluid Mech*. 1976;8(1):163–181.
35. Vermant J, Walker L, Moldenaers P, Mewis J. Orthogonal versus parallel superposition measurements. *J Non-Newton Fluid Mech.* 1998;79(2–3):173–189.
36. Kim S, Mewis J, Clasen C, Vermant J. Superposition rheometry of a wormlike micellar fluid. *Rheol Acta*. 2013;52(8-9): pp 727–740.

Manuscript received Jan. 21, 2014, and revision received Jan. 14, 2015.